

Single laser pulse driven thermal limit of the quasi-two dimensional magnetic ordering in Sr_2IrO_4

Ruitang Wang^{1,2,3}, J. Sun¹, D. Meyers^{4,5}, J. Q. Lin^{1,2,3}, J. Yang⁶, G. Li¹, H. Ding^{2,3}, Anthony D. DiChiara⁷, Y. Cao⁸, J. Liu⁶, M. P. M. Dean⁴, Haidan Wen^{7,8}, and X. Liu^{1*}

¹ *School of Physical Science and Technology, ShanghaiTech University, Shanghai 201210, China.*

² *Beijing National Laboratory for Condensed Matter Physics and Institute of Physics, Chinese Academy of Sciences, Beijing 100190, China*

³ *University of Chinese Academy of Sciences, Beijing 100049, China*

⁴ *Condensed Matter Physics and Materials Science Department, Brookhaven National Laboratory, Upton, New York 11973, USA.*

⁵ *Department of Physics, Oklahoma State University, Stillwater, Oklahoma 74078, USA.*

⁶ *Department of Physics and Astronomy, University of Tennessee, Knoxville, Tennessee 37996, USA.*

⁷ *Advanced Photon Source, Argonne National Laboratory, Argonne, IL, 60439, USA. and*

⁸ *Materials Science Division, Argonne National Laboratory, Argonne, Illinois, 60439, USA.*

Upon femtosecond-laser stimulation, generally materials are expected to recover back to their thermal-equilibrium conditions, with only a few exceptions reported. Here we demonstrate that deviation from the thermal-equilibrium pathway can be induced in canonical 3D antiferromagnetically (AFM) ordered Sr_2IrO_4 by a single 100-fs-laser pulse, appearing as losing long-range magnetic correlation along one direction into a glassy condition. We further discover a ‘critical-threshold ordering’ behavior for fluence above approximately 12 mJ/cm^2 which we show corresponds to the smallest thermodynamically stable c -axis correlation length needed to maintain long-range quasi-two-dimensional AFM order. We suggest that this behavior arises from the crystalline anisotropy of the magnetic-exchange parameters in Sr_2IrO_4 , whose strengths are associated with distinctly different timescales. As a result, they play out very differently in the ultrafast recovery processes, compared with the thermal equilibrium evolution. Thus, our observations are expected to be relevant to a wide range of problems in the nonequilibrium behavior of low-dimensional magnets and other related ordering phenomena.

I. INTRODUCTION

Understanding the mechanisms behind laser manipulation of magnetism in materials is indispensable to many problems in both fundamental and applied science [1–5]. Phenomenologically, the classic three-temperature model[5] works quite well in explaining the experimental observations on the evolution of the spins upon external femtosecond-laser stimuli in many systems[1, 5–8]. In this model, the spin, electron and lattice baths are coupled through a set of mutual interaction constants which govern the energy-flow rates when the system is stimulated into nonthermal equilibrium conditions. Eventually, the spin sector thermalizes back to equilibrium condition after the externally deposited energy equilibrates among the charge, spin and lattice reservoirs[5]. Here we report an exceptional observation of single-laser-pulse-induced anisotropic partial recovery of the magnetic ordering in Sr_2IrO_4 , leading to permanent reduction of the interplane magnetic correlation. We propose that this unusual recovery behavior could be explained by the non-cooperation of different terms of the exchange interactions dictating the spin ordering. When these exchanges differ significantly in strength, they are unfolded along the time axis[9, 10] into different time scales in the ultrafast recovery process. Because of this ‘time-window mis-

match’, the weaker exchange terms could be quenched, leading to a deviation from the quasiequilibrium relaxation pathway.

Sr_2IrO_4 is a layered Mott insulator with each Ir site hosting a $1/2$ pseudospin[11]. The highly anisotropic crystalline structure leads to strong magnetic anisotropy(Fig.1(a)). The system starts to develop three-dimensional antiferromagnetic(AFM) ordering below $T_N \sim 240 \text{ K}$ [12], from the cooperation of a strong intraplane exchange J of approximately 60 meV and a weak inter-plane exchange J_c of approximately $16 \mu\text{eV}$ [13, 14]. The magnetic ordering in Sr_2IrO_4 has been well observed with x-ray resonant magnetic scattering (XRMS) measurements, appearing as Bragg-peaks in the magnetic scattering channel when the incident x-ray energy is tuned to $\sim 11.216 \text{ keV}$ at the Ir- L_3 resonance edge[15]. This high x-ray resonant energy allows the access to a large reciprocal space, thus the flexibility in selecting low x-ray incident angle scattering geometry to best meet the x-ray and laser penetration match requirement[16, 17]. Our experiment was set up such that our $\sim 100 \text{ nm}$ epitaxial thin film sample was stimulated with 1 eV laser ($\sim 100 \text{ fs}$) pulse by pulse, and the AFM ordering peak was continuously monitored with XRMS at an x-ray incident angle of less than 5° to track the recovery of the magnetic ordering at a readout frequency of 1 Hz (see Ref. [18]).

* liuxr@shanghaitech.edu.cn

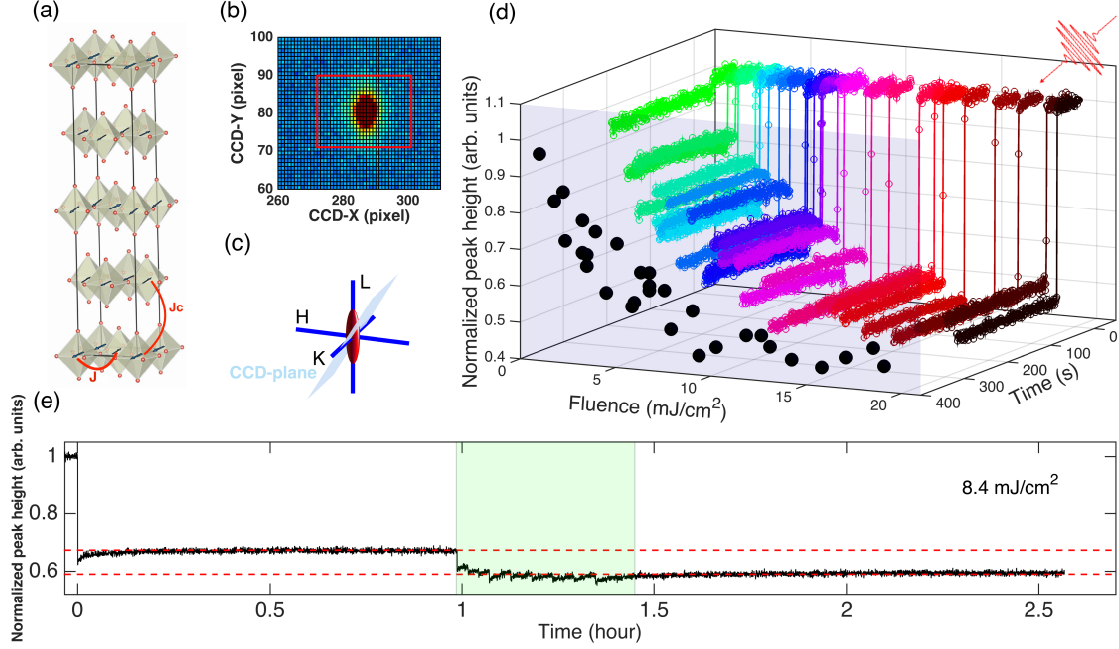


FIG. 1: Single-laser-pulse-induced suppression of the $(1\ 0\ 16)$ magnetic reflection. (a) The crystal and magnetic structure of Sr_2IrO_4 . J and J_c denote the in-plane and interplane exchange couplings, respectively. (b) CCD image of the magnetic peak. (c) Cartoon demonstration of the projection of the CCD plane in the reciprocal space. (d) Response of the magnetic Bragg-peak height to a single laser pulse (arrives at $t=0$) as a function of laser fluence. The black dots are the average of the last 100 s of each curve. (e) Multiple-shot evolution of the magnetic-peak height with moderate laser fluence. Multiple shots arrive in the shaded region and each creates a small intensity drop until the decrease is fully compensated by an initial recovery.

II. EXPERIMENTAL OBSERVATIONS

Figure 1(b) shows the $(1\ 0\ 16)$ 3D AFM ordering peak in Sr_2IrO_4 observed on the pixelated area detector at 80 K [19], and Fig. 1(c) depicts the detector surface projection in the reciprocal space. In order to catch the true first laser-shot response from pristine thermal-equilibrium condition, each dataset is collected after the sample goes through a fresh thermal cycle by warming above T_N and then cooling back again to 80 K with the laser turned off. Then x-ray is turned on to continuously monitor the magnetic Bragg-peak intensity. In between, laser stimuli are controlled to come in pulse by pulse. The arrival time of the first laser pulse is defined as time zero. The evolution of the experimentally observed magnetic-peak height as a function of the laser fluence is shown in Fig. 1(d).

After a single-laser-pulse stimulus to the magnetic ordering prepared from thermal-equilibrium evolution, the system does not recover to the initial state, evidenced by the permanent suppression of the magnetic Bragg-peak height as shown in Fig. 1(d). The degree of the suppression depends on the laser fluence, *i.e.*, the degree of the damage to the initial ordered spin network. More details

of the response to the pulsed laser stimulation are shown in Fig. 1(e) with a laser fluence of $8.4\ \text{mJ}/\text{cm}^2$. At this fluence, the first laser pulse leads to an approximately 33% drop in the magnetic Bragg-peak height, and the system settles at this condition without further evolution within an hour of continuous x-ray measurement. A second pulse arriving after one hour causes further suppression to the measured peak height, but with a much smaller drop. After 5~6 pulses, the system recovery becomes repeatable and more stimulation does not cause further permanent peak-height reduction.

These experimental observations clearly demonstrate that the recovery of the magnetic ordering in Sr_2IrO_4 depends on the history of laser stimulation, and the response can be classified into two distinct stages. In the first stage of the initial few pulses, the degree of magnetic ordering keeps to be permanently suppressed and the system does not recover to the condition before pulse arrival. In the second stage, the system does recover but only to a state prepared by multiple initial laser pulses, which, of course is different from the thermal-equilibrium evolution. The laser-pulse-induced suppression of the magnetic ordering can be erased with a full thermal cycle and our measurements are fully reproducible (see Ref. [18]),

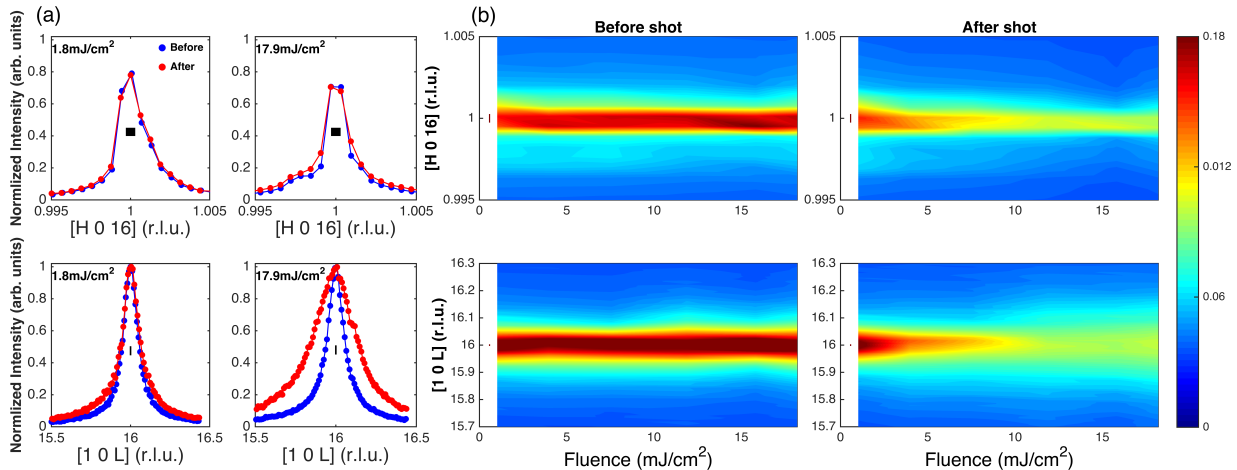


FIG. 2: Evolution of the magnetic ordering upon laser stimulation. (a) Comparison of the H (in-plane) and L (interplane) scans before and after single-pulse-laser pumping. The horizontal bars are our instrumental resolution. Scans are normalized to the peak height determined from L scans to emphasize the variation in the peak widths. (b) Fluence-dependence evolution of the H - and L - scans.

indicating the observed response is not due to sample damage but intrinsic to the spin system in Sr_2IrO_4 . Phenomenologically, the observed shot-by-shot dependence is similar to the photoinduced metastable insulator-to-metal phase transition in $\text{La}_{2/3}\text{Ca}_{1/3}\text{MnO}_3$ [20]. The laser stimulation drives the system into a nonthermal-equilibrium condition, and the deviation depends on the history of laser stimulation, a non-Markovian-type behavior. Such deviation is obviously beyond the classic three-temperature model [5–8].

To explore the microscopic origin of such evolution, detailed reciprocal space scans along the in-plane (H scans) and interplane (L scans) directions are performed across the magnetic peak before and after the first laser-pulse arrival under various laser fluences, and the results are shown in Fig. 2. Note that the peaks in the H scan, a measure of the in-plane spin ordering, are very sharp and identical before and after the laser pulses for all laser fluences applied. From the width of the peaks in H scans, the in-plane spin-ordering correlation length is estimated to be of a macroscopic scale about $0.9\ \mu\text{m}$. Thus, within a layer, the magnetic ordering is always fully restored to the thermal-equilibrium condition. The observed permanent suppression in the first stage is due to the incomplete recovery of the spin correlation along the interplane direction, which is evidenced by the broadening of the peaks in L scans. With the spin-correlation length reduced, the scattering intensity is transferred from the center to the tails, leading to a permanent suppression of the peak height as observed. These results suggest that the laser pulse leads to highly anisotropic response between the in-plane and interplane AFM ordering correlations in the recovery process.

To quantify such a response, the L scans of the mag-

netic Bragg peak measured at thermal-equilibrium condition and after the very first laser pulse stimulus with varying fluence were analyzed to extract the evolution of the interlayer spin-ordering texture. It turns out that, for all experimental conditions, the L scans can be well described by a single Lorentzian function as $I(q_z, \xi_z) \sim \frac{2}{d} \frac{\xi_z}{1+q_z^2 \xi_z^2}$ (Fig. 3(a,b), and Ref. [18]), with d to be the interlayer distance and q_z the interlayer direction relative-momentum transfer. The evolution of the extracted correlation length ξ_z is shown in Fig. 3(c). As a function of the laser fluence, ξ_z , as well as the peak height (Fig. 3(d)), generally follows an exponential decay. On the other hand, the total area under the magnetic peak is conserved (Fig. 3(e)). The significant data fluctuation mostly comes from slight misalignment in the H direction where the peak width corresponds to 0.01° in instrument rotational angle. Such conservation indicates that the size and direction of the local ordered magnetic moments are the same as those of the pristine condition [21, 22]. Thus the incomplete recovery is solely due to the reduction in the interplane correlation. It is interesting to notice that the exponential decay is offset from zero. Both the correlation length and the peak height show a tendency to saturation at higher laser fluence, and the interplane spin correlation cannot be completely destroyed.

III. DISCUSSION

Our observations reveal a few interesting aspects of the recovery of the magnetic-ordering texture in this highly magnetically anisotropic layered Sr_2IrO_4 . First, starting from the thermal-equilibrium condition, each of the first

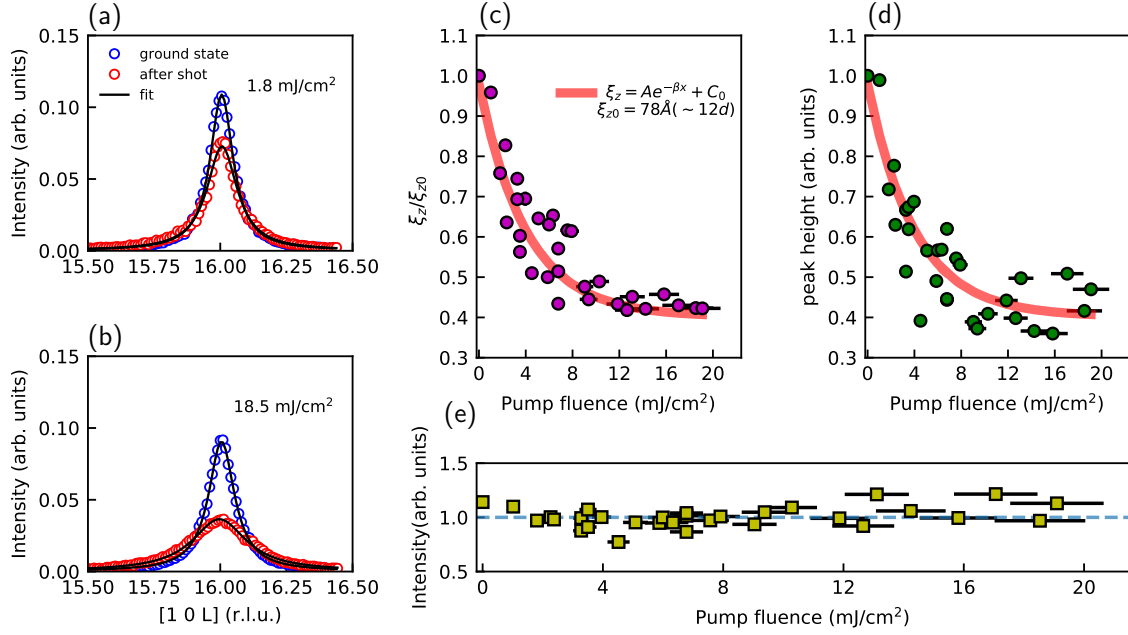


FIG. 3: Evolution of the interplane correlation as function of fluence. (a,b) The fitting results for two representative conditions with weak and strong laser fluence. (c-e) The evolution of the interplane correlation length ξ_z , peak height and the integrated intensity as function of fluence, which are all normalized to the values before laser stimulation. With fluence higher than ~ 12 mJ/cm², ξ_z saturates to ~ 5 layer thickness. The exponential lines are guides to the eye. The error bar for fluence is estimated to be 10%. (see Supplementary Material[18])

few femtosecond-laser pulses induces permanent suppression to the magnetic ordering, and the degree of the suppression depends on the states prepared by the preceding pulses. Second, the system does eventually stabilize into conditions that the recovery of the magnetism becomes repeatable upon consecutive laser stimulation. This justifies the validity of experiments of stroboscopic mode in probing the spin dynamics[1, 5, 17]. Third, although the degree of the partial recovery keeps degrading with increased laser fluence, it saturates to a robust nonzero value, indicating a minimum interplane partial recovery is intrinsically protected. The observed history and laser fluence- dependence hint at the nature of the magnetic recovery in Sr₂IrO₄ upon ultrafast laser stimulation.

The history dependence evidences that the demagnetization has certain local character. In the ultrafast process, the demagnetization does not completely wipe out all traces of magnetic order, and in the recovery the spins do not have long enough time to reach a global bath temperature. As a result, there are unperturbed (or less-perturbed) local spin clusters which preserve the memory of the prior state. Thus the prevailing global energy-dissipation picture in the classic three-temperature model[5–8] is oversimplified.

Notably, in both the initial and the second stages, the in-plane spin correlation always recovers to the thermal-equilibrium evolution condition of micron size. This differentiates our observation from the conventional fast quenching of a high-temperature state where the correla-

tions along all directions are expected to change[23–25]. The full in-plane recovery and the permanent loss of the interplane spin correlation are intimately related to the individual terms in the exchange interaction governing the magnetic dynamics along different directions. Although the 3D magnetic ordering in Sr₂IrO₄ is jointly determined by both the intraplane and interplane magnetic couplings [14, 26, 27], in the ultrafast recovery process they act differently. The strong in-plane exchange of tens of meV drives a quick re-establishment of the in-plane correlation within a few picoseconds[17]. We suggest that in a such short duration, the additional energy introduced by laser pumping into the spin system cannot be efficiently absorbed by the lattice reservoir[28, 29]. Instead, the spin sector is still highly excited in picosecond time scale. Associated with the weak interlayer exchange J_c of approximately 16 μ eV, a time window much longer than picoseconds is needed to allow them to fully dissipate. Such a process is cut off when the macroscopic intralayer spin correlation is established, since there is an enormous energy barrier to flip a whole layer.

Following the above arguments, we can understand the saturation plateau at high laser fluence as shown in Fig.3(c,d). In our earlier report[17], we have demonstrated that the laser pulse completely destroys the magnetic order in the initial hundreds of femtoseconds, when the laser fluence is stronger than approximately 12 mJ/cm². Thus, beyond such laser fluence, the system completely loses its memory of the history and

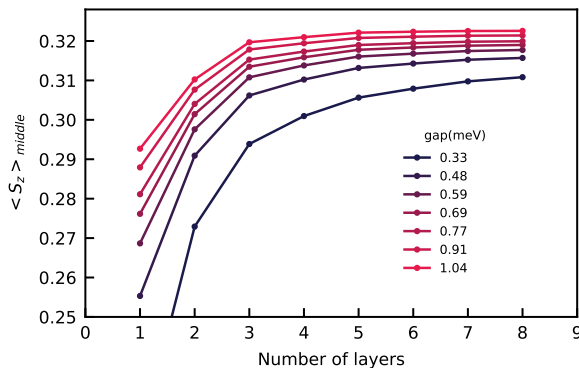


FIG. 4: Theoretical modeling. Calculated magnetic-order parameter at the middle of the slab, $\langle S_z \rangle_{middle}$, as a function of the layer number from the model Hamiltonian $H = \frac{J}{2} \sum_{l,ij} \vec{S}_{li} \cdot \vec{S}_{lj} + \Delta \sum_{l,ij} S_{li}^z S_{lj}^z + \frac{J_c}{2} \sum_{l',ij} \vec{S}_{li} \cdot \vec{S}_{l'j}$ at $T = 80$ K with exchange terms $J = 60$ meV, $J_c = 16.4$ μ eV. Different curves correspond to different anisotropic exchange Δ strengths, and the consequent gap sizes are used as an index.

the recovery follows the same path, regardless of further laser-fluence increasing. This is also consistent with the observed multishot evolution where, at high fluence, the laser pulses after the very first shot drive marginal further suppression to the magnetic Bragg-peak height (see Fig. S9 in Supplemental Material [18]). Without the assistance from the remnant order, reestablishment of the global interplane correlation completely lags behind the intraplane recovery. Thus the system recovery enters a quasi-two-dimensional regime. For such condition, Mermin and Wagner[30] prove that spontaneous two-dimensional ferromagnetic or antiferromagnetic long-range order at finite temperature is highly susceptible to spin thermal fluctuations, and the nonzero third-dimension correlation is critical to suppress the thermal fluctuation to realize long-range two-dimensional ordering.

We confirm such an explanation for our observed plateau by calculating the magnetic correlation function in a few layers of square lattice from an effective anisotropic Heisenberg spin-1/2 model, whose dynamics is solved with the equation-of-motion technique and mean-field approximation[31](see Ref. [18]). With the realistic parameters from experiment and published literature[13, 14], the self-consistent ordered magnetic moment $\langle S_z \rangle$ and the magnetic correlation function $\langle S^- S^+ \rangle$ are obtained as functions of the model slab thickness. As the reported exchange anisotropy for Sr_2IrO_4 is quite controversial[14, 32–34], the calculated $\langle S_z \rangle_{middle}$, the ordered magnetic moment at the middle of the slab, is shown in Fig.4 as a function of the calculated magnon gap size. As expected, both the anisotropic exchange Δ strengths and the layer thickness are critical for true

long-range magnetic ordering. When the gap size approaches approximately 1 meV, the magnetic-order parameter $\langle S_z \rangle_{middle}$ stabilizes around 4-5 layers, which agrees with the interplane correlation length of the saturation plateau we observe in experiment (Fig.3(c,d)). Thus, we realize a spin thermal fluctuation limit in real material with laser-pulse stimulation. Furthermore, this result indicates that indeed the interplane recovery-time window is set by the in-plane spin correlation. The longer interplane correlation established at lower fluence is assisted by memory of the spin network, which is only partially destroyed below the high-fluence threshold.

IV. CONCLUSION

In conclusion, a history and laser-fluence dependence of the partial-recovery process of the 3D AFM ordering in Sr_2IrO_4 was observed, which is related to the distinctly different timescales for the interplane and intraplane recoveries in the nonthermal-equilibrium ultrafast process. The noncooperation of the different exchange interactions in the ultrafast process drives the system to deviate from the quasiequilibrium relaxation pathway. Light-induced deviation from thermal-equilibrium evolution has been rarely observed, and previous reports are associated with the lattice[35] or charge[20, 36–38] degrees of freedom. Our results extend the direct observation of deviation from recovery to thermal-equilibrium condition into the spin sector. Furthermore, we suggest that such time-window mismatch could generally happen in complex systems during ultrafast nonthermal evolution, and our observations could be relevant to a wide range of problems in the nonequilibrium-behavior of low-dimensional magnets and related ordering phenomena. For example, the laser-induced ‘hidden quantum state’ in layered $1T\text{-TaS}_2$ could be one special case[38, 39].

V. ACKNOWLEDGMENTS

We thank Yi Zhu for the assistance of experimental setup. The experimental work by X. L. and R. W. was primarily supported by National Natural Science Foundation of China under grant No. 11934017. Part of the execution of the experiment and data interpretation by H. W. and Y. C. were supported by the U.S. DOE, Office of Science, Office of Basic Energy Sciences, Materials Sciences and Engineering Division. Use of the Advanced Photon Source was supported by the U.S. Department of Energy, Office of Science, Office of Basic Energy Sciences under contract No. DE-AC02-06CH11357. Work at Brookhaven National Laboratory was supported by the U.S. DOE, Office of Science, Office of Basic Energy Sciences, Materials Sciences and Engineering Division under Contract No. DE-SC0012704. J. L. acknowledges support from the National Science Foundation under Grant No. DMR-1848269. H. D. acknowledges sup-

port from the National Natural Science Foundation of China (No. 11888101). H. D. and X. L. acknowledge support from the Ministry of Science and Technology of China (2016YFA0401000). J. Y. acknowledges funding

from the State of Tennessee and Tennessee Higher Education Commission (THEC) through their support of the Center for Materials Processing.

-
- [1] A. Kirilyuk, A. V. Kimel, and T. Rasing, Ultrafast Optical Manipulation of Magnetic Order, *Rev. Mod. Phys.* 82, 2731 (2010).
 - [2] A.V. Kimel and M. Li, Writing Magnetic Memory with Ultrashort Light Pulses, *Nat. Rev. Mater.* 4, 189-200 (2019).
 - [3] J. Bigot, M. Vomir and E. Beaurepaire, Coherent ultrafast magnetism induced by femtosecond laser pulses, *Nat. Phys.* 5, 515 (2009).
 - [4] P. N  mec, M. Fiebig, T. Kampfrath and A. V. Kimel, Antiferromagnetic opto-spintronics, *Nat. Phys.* 14, 229 (2018).
 - [5] E. Beaurepaire, J.-C. Merle, A. Daunois, and J.-Y. Bigot, Ultrafast Spin Dynamics in Ferromagnetic Nickel, *Phys. Rev. Lett.* 76, 4250 (1996).
 - [6] Q. Zhang, A. V. Nurmikko, G. X. Miao, G. Xiao and A. Gupta, Ultrafast Spin-Dynamics in Half-Metallic CrO₂ Thin Flms. *Phys. Rev. B* 74, 064414 (2006).
 - [7] B. Koopmans, G. Malinowski, F. Dalla Longa, D. Steiauf, M. F  hnle, T. Roth, M. Cinchetti, and M. Aeschlimann, Explaining the Paradoxical Diversity of Ultrafast Laser-induced Demagnetization, *Nat. Mater.* 9, 259 (2010).
 - [8] J. Kimling, J. Kimling, R. B. Wilson, B. Hebler, M. Albrecht and D. G. Cahill, Ultrafast Demagnetization of FePt:Cu Thin Films and the Role of Magnetic Heat Capacity, *Phys. Rev. B* 90, 224408 (2014).
 - [9] M. Mitrano, et al., Ultrafast Time-resolved X-ray Scattering Reveals Diffusive Charge Order Dynamics in La_{2-x}Ba_xCuO₄, *Sci. Adv.* 5, eaax3346 (2019).
 - [10] C. Bostedt, S. Boutet, D. M. Fritz, Z. Huang, H. J. Lee, H. T. Lemke, A. Robert, W. F. Schlotter, J. J. Turner, and G. J. Williams, Linac Coherent Light Source: The First Five Years, *Rev. Mod. Phys.* 88, 015007 (2016).
 - [11] B. J. Kim, H. Jin, S. J. Moon, J.-Y. Kim, B.-G. Park, C. S. Leem, J. Yu, T. W. Noh, C. Kim, S.-J. Oh J.-H. Park, V. Durairaj, G. Cao, and E. Rotenberg, Novel $J_{eff}=1/2$ Mott State Induced by Relativistic Spin-Orbit Coupling in Sr₂IrO₄, *Phys. Rev. Lett.* 101, 076402 (2008).
 - [12] M. K. Crawford, M. A. Subramanian, R. L. Harlow, J. A. Fernandez-Baca, Z. R. Wang, and D. C. Johnston, Structural and Magnetic Studies of Sr₂IrO₄, *Phys. Rev. B* 49, 9198 (1994).
 - [13] J. Kim, D. Casa, M. H. Upton, T. Gog, Y.-J. Kim, J. F. Mitchell, M. van Veenendaal, M. Daghofer, J. van den Brink, G. Khaliullin, and B. J. Kim, Magnetic Excitation Spectra of Sr₂IrO₄ Probed by Resonant Inelastic X-Ray Scattering: Establishing Links to Cuprate Superconductors, *Phys. Rev. Lett.* 108, 177003 (2012).
 - [14] J. Porras, J. Bertinshaw, H. Liu, G. Khaliullin, N. H. Sung, J.-W. Kim, S. Francoual, P. Steffens, G. Deng, M. Moretti Sala, A. Efimenko, A. Said, D. Casa, X. Huang, T. Gog, J. Kim, B. Keimer, and B. J. Kim, Pseudospin-lattice Coupling in the Spin-Orbit Mott Insulator Sr₂IrO₄, *Phys. Rev. B* 99, 085125 (2019).
 - [15] B. J. Kim, H. Ohsumi, T. Komesu, S. Sakai, T. Morita, H. Takagi, and T.-H. Arima, Phase-Sensitive Observation of a Spin-Orbital Mott State in Sr₂IrO₄, *Science* 323, 1329 (2009).
 - [16] B. Guzelturk, T. Winkler, T. W. J. Van de Goor, M. D. Smith, S. A. Bourelle, S. Feldmann, M. Trigo, S. W. Teitelbaum, H. G. Steinr  ck, G. A. de la Pena, R. Alonso-Mori, D. Zhu, T. Sato, H. I. Karunadasa, M. F. Toney, F. Deschler, and A. M. Lindenberg, Visualization of Dynamic Polaronic Strain Fields in Hybrid Lead Halide Perovskites, *Nat. Mater.* 20, 618 (2021).
 - [17] M. Dean, Y. Cao, X. Liu, S. Wall, D. Zhu, R. Mankowsky, V. Thampy, X. M. Chen, J. G. Vale, D. Casa et al., Ultrafast Energy- and Momentum-Resolved Dynamics of Magnetic Correlations in the Photo-Doped Mott Insulator Sr₂IrO₄, *Nat. Mater.* 15, 601 (2016).
 - [18] (see Supplemental Material.)
 - [19] A. Lupascu, J.P. Clancy, H. Gretarsson, Z. Nie, J. Nichols, J. Terzic, G. Cao, S. S. A. Seo, Z. Islam, M. H. Upton, Jungho Kim, D. Casa, T. Gog, A. H. Said, V.M. Katukuri, H. Stoll, L. Hozoi, J. van den Brink, and Y.-J. Kim, Tuning Magnetic Coupling in Sr₂IrO₄ Thin Films with Epitaxial Strain, *Phys. Rev. Lett.* 112, 147201 (2014).
 - [20] J. Zhang, X. Tan, M. Liu, S. W. Teitelbaum, K. W. Post, F. Jin, K. A. Nelson, D. Basov, W. Wu, and R. D. Averitt, Cooperative Photoinduced Metastable Phase Control in Strained Manganite Films, *Nat. Mater.* 15, 956 (2016).
 - [21] M. F. Collins, *Magnetic Critical Scattering* (Oxford University Press, 1989).
 - [22] R. F. Shannon, S. E. Nagler, C. R. Harkless, and R. M. Nicklow, X-Ray Intensity Fluctuation Spectroscopy Studies on Phase-Ordering Systems, *Phys. Rev. B* 46, 40 (1992).
 - [23] A. J. Bray, Theory of Phase-Ordering Kinetics, *Adv. Phys.* 43, 357 (1994).
 - [24] G. F. Mazenko, Theory of Unstable Growth, *Phys. Rev. B* 42, 4487 (1990).
 - [25] P. J. Shah and O. G. Mouritsen, Dynamics of Ordering Processes in Annealed Dilute Systems: Island Formation, Vacancies at Domain Boundaries, and Compactification, *Phys. Rev. B* 41, 7003 (1990).
 - [26] M. A. Kastner, R. J. Birgeneau, G. Shirane, and Y. Endoh, Magnetic, Transport, and Optical Properties of Monolayer Copper Oxides, *Rev. Mod. Phys.* 70, 897 (1998).
 - [27] S. Fujiyama, H. Ohsumi, T. Komesu, J. Matsuno, B. J. Kim, M. Takata, T. Arima, and H. Takagi, Two-Dimensional Heisenberg Behavior of $J_{eff}=1/2$ Isospins in the Paramagnetic State of the Spin-Orbital Mott Insulator Sr₂IrO₄, *Phys. Rev. Lett.* 108, 247212 (2012).
 - [28] J. Li, R. Wang, H. Guo, Y. Zhu, Y. Cao, J. Liu, H. Ding, H. Wen and X. Liu, Recovery of Photoexcited Magnetic Ordering in Sr₂IrO₄. *J. Phys.: Condens. Matter* 31 25580

- (2019).
- [29] Y. Li, R. D. Schaller, M. Zhu, D. A. Walko, J. Kim, X. Ke, L. Miao and Z. Q. Mao, Strong Lattice Correlation of Non-Equilibrium Quasiparticles in a Pseudospin-1/2 Mott Insulator Sr_2IrO_4 , *Sci. Rep.* 6, 19302 (2016).
 - [30] N. Mermin, and H. Wagner, Absence of Ferromagnetism or Antiferromagnetism in One- or Two-Dimensional Isotropic Heisenberg Models, *Phys. Rev. Lett.* 17, 1133 (1966).
 - [31] H. Diep, Quantum Effects in Heisenberg Antiferromagnetic thin Films, *Phys. Rev. B* 43, 8509 (1991)
 - [32] Y. Gim, A. Sethi, Q. Zhao, J. F. Mitchell, G. Cao, and S. L. Cooper, Isotropic and Anisotropic Regimes of the Field-Dependent Spin Dynamics in Sr_2IrO_4 : Raman Scattering Studies, *Phys. Rev. B* 93, 024405 (2016).
 - [33] S. Calder, D. M. Pajerowski, M. B. Stone, and A. F. May, Spin-gap and Two-Dimensional Magnetic Excitations in Sr_2IrO_4 , *Phys. Rev. B* 98, 220402(R) (2018).
 - [34] D. Pincini, J. G. Vale, C. Donnerer, A. de la Torre, E. C. Hunter, R. Perry, M. Moretti Sala, F. Baumberger, and D. F. McMorrow, Anisotropic Exchange and Spin-Wave Damping in Pure and Electron-Doped Sr_2IrO_4 , *Phys. Rev. B* 96, 075162 (2017).
 - [35] V. A. Stoica, N. Laanait, C. Dai et al., Optical Creation of a Supercrystal with Three-Dimensional Nanoscale Periodicity, *Nat. Mater.* 18, 377 (2019).
 - [36] V. Kiryukhin, D. Casa, J. Hill, B. Keimer, A. Vigliante, Y. Tomioka and Y. Tokura, An X-Ray-Induced Insulator-Metal Transition in a Magnetoresistive Manganite, *Nature* 386, 813 (1997).
 - [37] S.-Y. Xu, Q. Ma, Y. Gao, A. Kogar, A. Zong, A. M. M. Valdivia, T. H. Dinh, S.-M. Huang, B. Singh, C.-H. Hsu et al., Spontaneous Gyrotropic Electronic Order in a Transition-Metal Dichalcogenide, *Nature (London)* 578, 545 (2020).
 - [38] L. Stojchevska, I. Vaskivskyi, T. Mertelj, P. Kusar, D. Svetin, S. Brazovskii and D. Mihailovic, Ultrafast Switching to a Stable Hidden Quantum State in an Electronic Crystal, *Science* 344, 177 (2014).
 - [39] S.-H. Lee, J. S. Goh and D. Cho, Origin of the Insulating Phase and First-order Metal-Insulator Transition in 1T-TaS₂, *Phys. Rev. Lett.* 122, 106404 (2019).

Supplemental material for “Single Laser Pulse Driven Thermal Limit of the Quasi-Two Dimensional Magnetic Ordering in Sr_2IrO_4 ”

Ruitang Wang^{1,2,3}, J. Sun¹, D. Meyers^{4,5}, J. Q. Lin^{1,2,3}, J. Yang⁶, G. Li¹, H. Ding^{2,3}, Anthony D. DiChiara⁷, Y. Cao⁸, J. Liu⁶, M. P. M. Dean⁴, Haidan Wen^{7,8}, and X. Liu^{1*}

¹ School of Physical Science and Technology, ShanghaiTech University, Shanghai 201210, China.

² Beijing National Laboratory for Condensed Matter Physics and Institute of Physics, Chinese Academy of Sciences, Beijing 100190, China

³ University of Chinese Academy of Sciences, Beijing 100049, China

⁴ Condensed Matter Physics and Materials Science Department, Brookhaven National Laboratory, Upton, New York 11973, USA.

⁵ Department of Physics, Oklahoma State University, Stillwater, Oklahoma 74078, USA.

⁶ Department of Physics and Astronomy, University of Tennessee, Knoxville, Tennessee 37996, USA.

⁷ Advanced Photon Source, Argonne National Laboratory, Argonne, IL, 60439, USA. and

⁸ Materials Science Division, Argonne National Laboratory, Argonne, Illinois, 60439, USA.

I. SAMPLE SYNTHESIS AND CHARACTERIZATION

Sr_2IrO_4 thin film samples with thickness of ~ 100 nm grown with PLD method were used[1]. Sr_2IrO_4 is crystallized in $I4_1/acd$ structure with single IrO_2 layers separated by SrO layers[2]. Each structural unit cell contains two Ir in one layer and four IrO_2 layers along c direction. The antiferromagnetic (AFM) ordering sets in at $T_N \approx 240\text{K}$ for bulk crystal. In our thin film samples, the magnetic susceptibility measurement gave slightly lower T_N as shown in **Fig. S1**. The AFM ordering shares the same unit cell at that of the structure[3]. In the tetragonal Sr_2IrO_4 , two twined magnetic domains are expected to produce two sets of magnetic reflection peaks at $(1\ 0\ 4n)$, $(0\ 1\ 4n+2)$ and $(1\ 0\ 4n+2)$, $(0\ 1\ 4n)$ respectively, where lattice reflections are forbidden. The magnetic ordering peaks from both domains were observed in the long range L-scan shown in **Fig. S2**, which are at $(1\ 0$

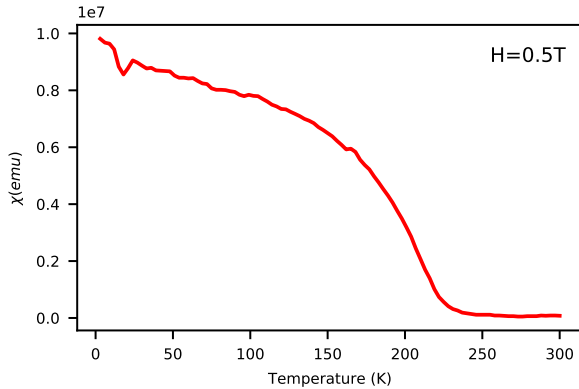


Fig. S 1: Temperature dependence of the magnetic susceptibility of our Sr_2IrO_4 thin film sample.

16) and $(1\ 0\ 18)$ respectively. Importantly, both peaks respond to laser stimulation in the same way.

II. CHARACTERIZATION OF LASER SPOT AND ESTIMATION OF THE EFFECTIVE AVERAGE FLUENCE

Discrete laser pulses with a duration of ~ 100 fs was used to pump the sample. The pump laser photon energy was selected to be 1 eV derived from a Ti: Sapphire laser system with an optical parametric amplifier, corresponding to the resonant excitation from $J_{eff} = \frac{3}{2}$ to unoccupied $J_{eff} = \frac{1}{2}$ states [4]. Thus the pumping largely creates double occupancy of the $J_{eff} = \frac{1}{2}$ states and leaves a hole in the $J_{eff} = \frac{3}{2}$ manifold. We have shown that 1eV pumping can efficiently break the long range AFM ordering[5]. The laser system runs at 1 KHz and can be controlled to deliver a single-shot laser pulse on demand.

To properly characterize the laser fluence, the laser power density profile was measured, as shown in **Fig. S3**. The profile can be modeled as an isotropic Gaussian pulse with the fitted σ to be $350\mu\text{m}$. In the experiment, the laser incident angle was 47° . Thus the laser on-sample footprint was elongated along one direction with $\sigma' = \sigma/\sin(47^\circ) = 479\mu\text{m}$. The effective laser fluence under the X-ray spot can be calculated as,

$$F = \frac{P}{A_f} \iint_A \frac{1}{2\pi\sigma\sigma'} \exp\left[-\left(\frac{x^2}{\sigma^2} + \frac{y^2}{\sigma'^2}\right)\right] dx dy \quad (1)$$

where A is the overlapped area of the X-ray at the laser spot center on the sample surface, f is the running frequency as 1 kHz, and P is the laser power measured during the experiments. At $P = 1\text{mW}$ with $A = 2.41 \times 10^{-4}\text{cm}^2$, the average fluence within the overlapped region of the single laser shot and X-ray beam spot on the sample is 0.113 mJ/cm^2 . As the X-ray to the laser spot center overlap was done by referring to a video camera monitor, we expect certain miss-alignment.

* liuxr@shanghaitech.edu.cn

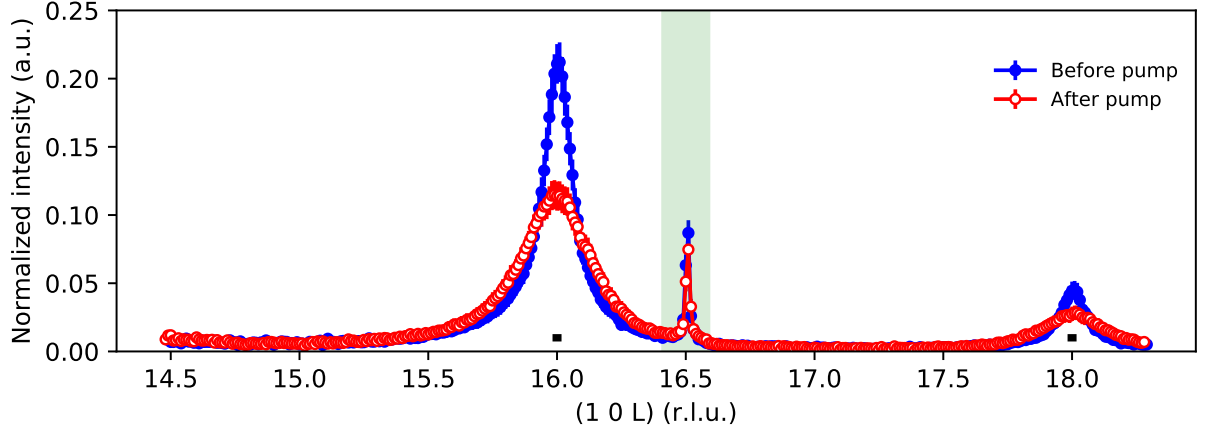


Fig. S 2: Long-range L-scan of (1 0 L) magnetic Bragg peaks along c-axis direction. The long-range reciprocal space scan along out-of-plane direction(L scan) was performed for pristine thermal equilibrium condition of the sample at 80K(blue) and after the first single laser shot(red). The appearance of both (1 0 16) and (1 0 18) magnetic Bragg peaks indicate the existence of twinned magnetic domains $[(1\ 0\ 4n), (0\ 1\ 4n+2)]$ and $[(1\ 0\ 4n+2), (0\ 1\ 4n)]$ in our sample. Both of these two magnetic domains respond to the single shot in a similar manner. The horizontal small bars represents the instrumental resolution. The peak at $L = 16.5$ (marked by the shaded region) comes from the $(\frac{1}{2}\ \frac{1}{2}\ \frac{5}{2})$ superlattice peak of the SrTiO_3 substrate.

In **Fig. 3** in the main text, the error bar given for fluence is 10% by assuming possible $\pm 60\mu\text{m}$ miss-alignment.

At $\sim 1\text{eV}$, the penetration depth of the pumping laser for Sr_2IrO_4 is estimated[5] to be $\sim 100\text{ nm}$.

III. SCHEMATIC OF EXPERIMENT

The X-ray resonant magnetic scattering(XRMS) measurements were conducted at the Advanced Photon Sources(APS) using beamline 7-ID-C. The data were collected at Ir L_3 absorption edge of 11.216 KeV. A horizontal scattering geometry was used.(see **Fig. S4**) The laser pulse came in at a large angle of 47° relative to the sample surface to allow a more homogeneous excitation along the sample depth direction.

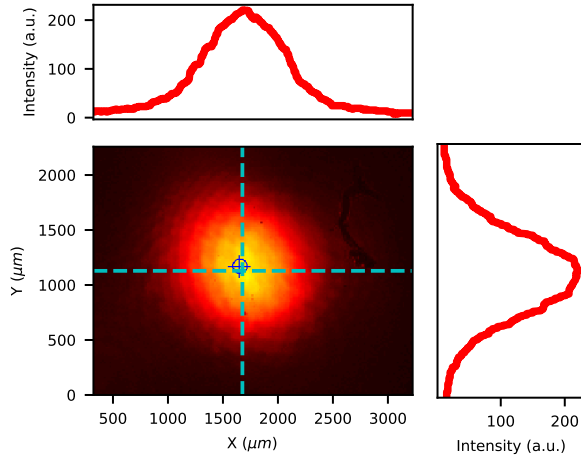


Fig. S 3: Characterization of the laser spot size. The energy density profile of the pump laser was measured with CCD, as shown in the image. Two line cuts (shown by the dashed lines in the CCD image) were taken to extract the peak widths. From Gaussian fitting, both directions give $\sigma = 350\mu\text{m}$.

To amplify the magnetic scattering signal[6], the scattering experiment was performed in the a - c plane with the incident X-ray came in at a shallow angle of 4.87° relative to the sample surface. Its polarization was almost parallel to the sample surface c -direction. A Pilatus CCD with pixel size of $172\ \mu\text{m}^2$ was used in the experiment to monitor the scattered X-ray signal. It was placed $\sim 1\text{m}$ away from the sample, which gives an angular resolution of 0.01° per pixel. The sample was cooled down to 80 K with cryostat, well below the Néel ordering temperature. During the experiment, a full thermal cycle was done by warming the sample up to 280 K and then slowly cooling down to 80 K with a cooling rate of 0.05 K/s. The laser induced suppression of the magnetic peak height was fully recovered after a thermal cycle, as shown in the cross-sample scan in **Fig. S5**. The entire process is repeatable, ruling out the irreversible sample damage issue.

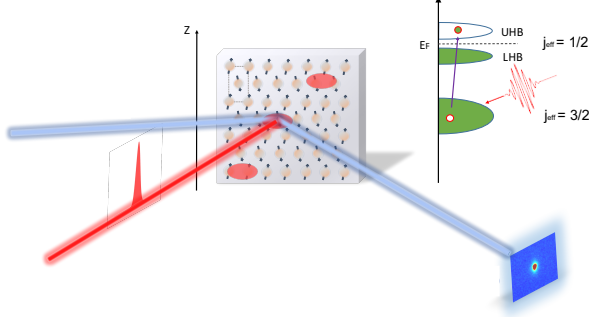


Fig. S 4: Experimental configuration. The XRMS experiment was performed in a horizontal scattering geometry where the a - and c -axis of sample lie within the scattering plane. Three far-apart separated spots on the sample were chosen to be measured in between slow thermal-cycle processes to save experimental time. The inset shows the corresponding electron excitations from laser pumping, where 1 eV laser pulses mainly drive electrons from $J_{eff} = \frac{3}{2}$ states into the unoccupied $J_{eff} = \frac{1}{2}$ states.

IV. LASER EFFECT ON STRUCTURAL PEAK

To check the laser shot effect on the crystal structure, (0 0 16) structure peak height was monitored with single laser pulse stimulation. As shown in **Fig. S6**, the fluctuation in the structural peak height, mainly due to X-ray beam instability, is uncorrelated with the laser stimulation. Thus laser induces minimum effect to the lattice at 1Hz frequency of which our data was taken, and the suppression of the magnetic peak height is intrinsic to the spin sector.

V. X-RAY EFFECT ON MAGNETIC PEAK

We checked the X-ray effect on magnetic peak by monitoring the (1 0 16) magnetic Bragg peak height after X-ray was initially turned on after a full thermal cycle, without any optical pumping on sample. A gradual reduction of the peak height about 7% was noticed after the X-ray exposure of the sample, as shown in **Fig. S7**. Then the peak height stabilized after a few minutes.

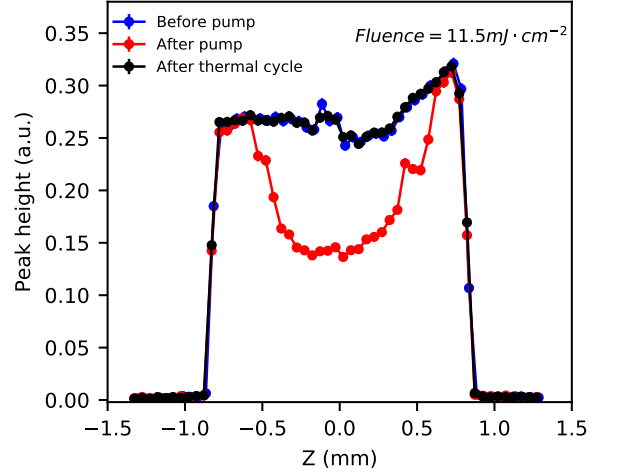


Fig. S 5: Cross-sample scan. Real space scans along z -direction (see the experimental schematic in **Fig. S4**) across the sample while monitoring the (1 0 16) magnetic peak height. Three scans were taken for: pristine thermal equilibrium condition (blue curve), after single laser pulse excitation (red curve), and after a full thermal cycle process (black curve). The laser pumping leads to a drastic suppression of the scattering intensity, which is fully recovered after a thermal cycle.

VI. FORMULA FOR THE DIFFRACTION PROFILE OF THE L-SCAN OF MAGNETIC BRAGG PEAK

Since the in-plane AFM ordering correlation length is fully restored, we focus on the inter-plane correlation. A phenomenological model is constructed by assuming

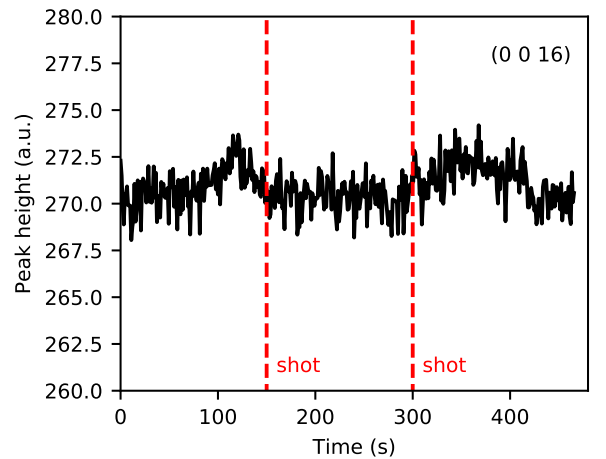


Fig. S 6: Laser effect on structural peak. response of the (0 0 16) structural Bragg peak height to laser stimulation. The dashed lines mark two single laser pulses.

the AFM ordered iso-spins are still pointing to the crystal a -direction as in the thermal equilibrium state while their inter-plane correlation is described by an exponential decay as $e^{-\frac{|z_m - z_n|}{\xi}}$ with $z_{m(n)}$ to be the c -direction

coordinate. Accordingly, the magnetic reflection intensity can be written as,

$$I(Q_z, \xi_z) = |F|^2 \left[\delta(Q_x - h \cdot a^*) \delta(Q_y - k \cdot b^*) \right]^2 \cdot \frac{1}{N_3} \sum_{j,k=1}^{N_3} (-1)^j e^{-iQ_z z_j} (-1)^k e^{iQ_z z_k} e^{-\frac{|z_j - z_k|}{\xi_z}} \quad (2)$$

where F is the magnetic scattering factor for Ir sites, and j and k represents the j -th and k -th plane along c -direction. N_3 is the total plane number along c -direction. ξ_z is the c -direction magnetic correlation length. The in-plane structure factors are simplified to δ -functions due to the fact that the in-plane correlation lengths are orders of magnitude larger than the c -direction correlation length (see main text). The summation can be analytically carried out as:

$$I(Q_z, \xi_z) = |F|^2 \frac{\sinh(\frac{d}{\xi_z})}{\cosh(\frac{d}{\xi_z}) - \cos(Q_z d)} \quad (3)$$

where d is the inter-layer distance.

The relative momentum transfer can be defined as $q_z = Q_z - G$ with G indexing the Bragg points. When $\frac{(q_z d)^4}{4!} \ll 1$, close to the Bragg point as where our L -scans were taken, Eqn. 3 can be simplified as:

$$I(q_z, \xi_z) = |F|^2 \frac{\sinh(\frac{d}{\xi_z})}{\cosh(\frac{d}{\xi_z}) - \cos(q_z d)} \quad (4)$$

$$\approx |F|^2 \frac{(\frac{d}{\xi_z})}{\frac{d^2}{2\xi_z^2} + \frac{(q_z)^2}{2}} \quad (5)$$

$$= |F|^2 \frac{2}{d} \frac{\xi_z}{1 + q_z^2 \xi_z^2} \quad (6)$$

Thus, with inter-layer ordering correlation defined as $e^{-\frac{|z_m - z_n|}{\xi_z}}$, the X-ray scattering profile is of a Lorentzian shape. The peak height at $q_z = 0$ should be proportional to the correlation length ξ_z , while the whole integrated intensity is constant. All these predictions agree well with our observations, suggesting a quite homogeneous statistical distribution of the c -direction spin ordering.

VII. FITTING PROCEDURE OF THE MAGNETIC BRAGG PEAK

All the magnetic peaks were fitted based on the Eqn. 6 plus a linear background intensity, as shown in Eqn. 7. For a set of magnetic Bragg peaks studied with the same fluence of laser pulse, firstly we fit the magnetic Bragg peaks of pristine thermal limit (before laser excitation), and extract a background intensity; Then we fit the magnetic Bragg peaks after the single shot excitation with the same background intensity. (see **Fig. S8b**)

$$I(q_z, h, \xi_z) = \frac{2}{d} \frac{h}{1 + q_z^2 \xi_z^2} + I_{bg} \quad (7)$$

The fitting was done by least-squares fitting. And here the reduced Chi-square χ_ν^2 is defined as:

$$\chi_\nu^2 = \frac{1}{N - N_{vars}} \sum_i^N \frac{[y_i^{exp} - y_i^{model}(v)]^2}{\epsilon_i^2} \quad (8)$$

where N is the number of data points, N_{vars} is the number of variables in the fit, y_i^{exp} is the measured data, $y_i^{model}(v)$ is the model calculation and v is the set of variables in the model to be optimized in the fit, and ϵ_i is the estimated uncertainty in the data.

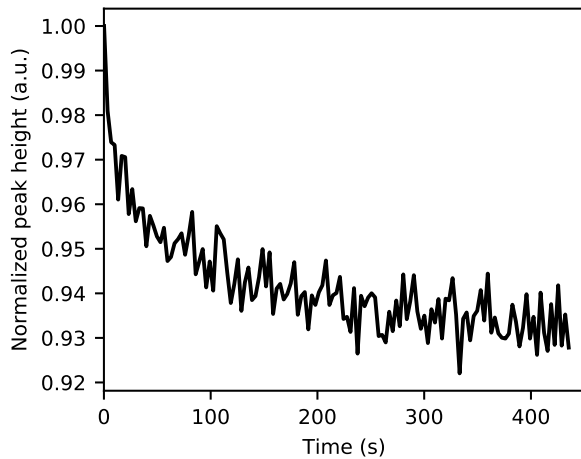


Fig.S 7: X-ray effect on magnetic peak. Temporal evolution of the (1 0 16) magnetic Bragg peak height (normalized) in the initial 420 seconds after turning on the X-ray.

TABLE I: Fitting goodness

Fluence(mJ/cm^2)	1.0	3.3	6.0	6.8	9.4	11.9	13.1	18.5
χ^2_ν	18.4	21.6	30.7	8.5	4.9	8.7	6.8	6.2

Representative fitting goodness is listed in Table. SI. And we plot three of the typical fitting results in **Fig. S8a**.

VIII. MULTIPLE SHOTS EVOLUTION OF THE MAGNETIC PEAK HEIGHT

Magnetic peak height was measured upon a sequence of laser shots of various fluences. As shown in **Fig. S9**, each of the first a few shots induced certain degree of suppression to the magnetic peak height. After those initial shots, the peak height does fully recover, but only to a reduced level prepared by the initial multiple pulses. The stabilized conditions are obviously dependent on the laser pulse fluence.

IX. MODELING THE THICKNESS DEPENDENCE OF THE AFM ORDERING AT FINITE TEMPERATURE

We evaluate the saturation of the low limit of the observed inter-plane correlation by considering a minimum Quasi-2D spin model. As shown in **Fig. S10**, spin-1/2 objects are placed at the Ir sites which are AFM ordered, forming spin-up (A) and spin-down (B) sublattices. The exchange interactions considered are: the nearest-neighbor in-plane AFM exchange J , the inter-plane next-nearest-neighbor exchange J_{1c} and J_{2c} for the coupling within and between the spin-up and spin-down sublattices. Also, the anisotropy of the nearest-neighbor exchange, Δ , is considered. As a result, the Hamiltonian for this minimum spin model can be written as[7, 8],

$$\begin{aligned}
H &= \frac{J}{2} \sum_{l<ij>} \vec{S}_{li} \cdot \vec{S}_{lj} + \Delta \sum_{l<ij>} S_{li}^z S_{lj}^z + \frac{J_c}{2} \sum_{<ll'><ij>} \vec{S}_{li} \cdot \vec{S}_{l'j} \\
&= \frac{J}{2} [D \sum_{l<ij>} S_{lAi}^z S_{lBj}^z + \frac{1}{2} \sum_{l<ij>} (S_{lAi}^+ S_{lBj}^- + S_{lAi}^- S_{lBj}^+)] \\
&\quad + J [D \sum_{l<ij>} S_{lBi}^z S_{lAj}^z + \frac{1}{2} \sum_{l<ij>} (S_{lBi}^+ S_{lAj}^- + S_{lBi}^- S_{lAj}^+)] \\
&\quad + \frac{J_{1c}}{2} [\sum_{<ll'>} \sum_{<ij>} S_{lAi}^z S_{l' Aj}^z + \frac{1}{2} \sum_{<ll'>} \sum_{<ij>} (S_{lAi}^+ S_{l' Aj}^- + S_{lAi}^- S_{l' Aj}^+)] \\
&\quad + \frac{J_{1c}}{2} [\sum_{<ll'>} \sum_{<ij>} S_{lBi}^z S_{l' Bj}^z + \frac{1}{2} \sum_{<ll'>} \sum_{<ij>} (S_{lBi}^+ S_{l' Bj}^- + S_{lBi}^- S_{l' Bj}^+)] \\
&\quad + \frac{J_{2c}}{2} [\sum_{<ll'>} \sum_{<ij>} S_{lAi}^z S_{l' Bj}^z + \frac{1}{2} \sum_{<ll'>} \sum_{<ij>} (S_{lAi}^+ S_{l' Bj}^- + S_{lAi}^- S_{l' Bj}^+)] \\
&\quad + \frac{J_{2c}}{2} [\sum_{<ll'>} \sum_{<ij>} S_{lBi}^z S_{l' Aj}^z + \frac{1}{2} \sum_{<ll'>} \sum_{<ij>} (S_{lBi}^+ S_{l' Aj}^- + S_{lBi}^- S_{l' Aj}^+)]
\end{aligned} \tag{9}$$

where D is defined as $D = 1 + \Delta$.

To compare with our experimental observations on Sr_2IrO_4 , we refer to the published literature[9–11] and set,

- Nearest neighbor exchange interaction $J = 60 \text{ meV}$
- Interlayer exchange interaction: within the same sublattice $J_{1c} = -16.4 \text{ } \mu\text{eV}$; between the two sublattices $J_{2c} = 16.4 \text{ } \mu\text{eV}$

- the anisotropic term related to the magnon gap as $E(k) = ZJ\langle Sz \rangle \sqrt{D^2 - \gamma_k^2}$

As the reported exchange anisotropy for Sr_2IrO_4 is quite controversial[9–13], the gap size was carried as a free parameter in our calculation. The dynamics of the above Hamiltonian was solved with the equation of motion technique and mean-field approximation for model systems with different thickness.

Using the equation of motion of double-time Green's function[7, 8, 14], we can obtain a set of Green's functions for each layer:

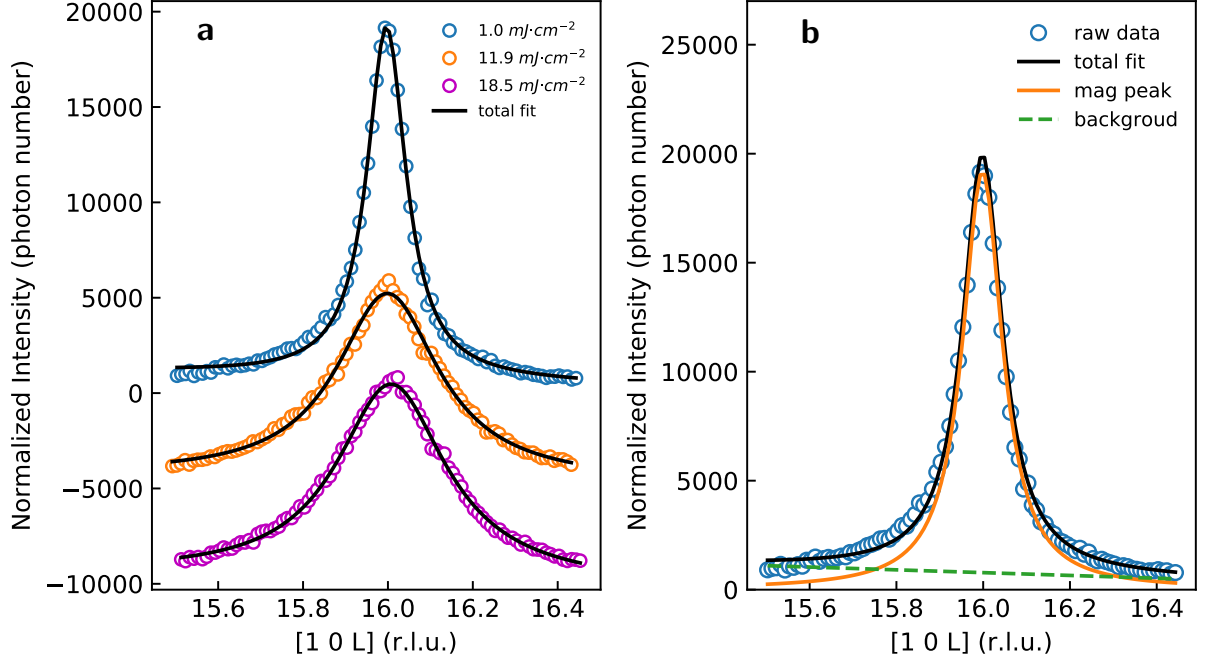


Fig. S 8: **Fitting Procedure of Magnetic Bragg Peak:** All the magnetic Bragg peaks were fitted with the Lorentzian function we derived with a linear background(Eqn. 7) using the least-squares fitting method. **a**, Three L-scan data after laser excitation and the fitting results (vertically stacked for clarity). **b**, The fitting components of a typical L-scan data.

$$\begin{aligned}
& [\omega - JDZ\langle S_l^z \rangle + Z'(J_{1c} - J_{2c})(\langle S_{l+1}^z \rangle + \langle S_{l-1}^z \rangle)]g_{ll} - J\langle S_l^z \rangle Z\gamma(k)f_{ll} \\
& - J_{1c}Z'\gamma_{AA}(k)(g_{l-1,l}(k) + g_{l+1,l}(k)) - J_{2c}Z'\gamma_{AB}(k)(f_{l-1,l}(k) + f_{l+1,l}(k)) = 2\langle S_l^z \rangle \\
& [\omega + JDZ\langle S_l^z \rangle - Z'(J_{1c} - J_{2c})(\langle S_{l+1}^z \rangle + \langle S_{l-1}^z \rangle)]f_{ll} + J\langle S_l^z \rangle Z\gamma(k)g_{ll} \\
& + J_{1c}Z'\gamma_{AA}(k)(f_{l-1,l}(k) + f_{l+1,l}(k)) + J_{2c}Z'\gamma_{AB}(k)(g_{l-1,l}(k) + g_{l+1,l}(k)) = 0 \\
& [\omega - JDZ\langle S_{l-1}^z \rangle + Z'(J_{1c} - J_{2c})(\langle S_l^z \rangle + \langle S_{l-2}^z \rangle)]g_{l-1,l} - J\langle S_{l-1}^z \rangle Z\gamma(k)f_{l-1,l} \\
& - J_{1c}Z'\gamma_{AA}(k)\langle S_{l-1}^z \rangle(g_{l-2,l}(k) + g_{l,l}(k)) - J_{2c}Z'\gamma_{AB}(k)\langle S_{l-1}^z \rangle(f_{l-2,l}(k) + f_{l,l}(k)) = 0 \\
& [\omega + JDZ\langle S_{l-1}^z \rangle - Z'(J_{1c} - J_{2c})(\langle S_{l-2}^z \rangle + \langle S_l^z \rangle)]f_{l-1,l} + J\langle S_{l-1}^z \rangle Z'\gamma(k)g_{l-1,l} \\
& + J_{1c}Z'\gamma_{AA}(k)\langle S_{l-1}^z \rangle(f_{l-2,l}(k) + f_{l,l}(k)) + J_{2c}Z'\gamma_{AB}(k)\langle S_{l-1}^z \rangle(g_{l,l-2}(k) + g_{l,l}(k)) = 0
\end{aligned} \tag{10}$$

Where N is the total number of layers, and l is the index of each layer ($l = 1, 2, \dots, N$). Z, Z' are the in-plane and out of plane coordinate numbers. $g_{ll}(k)$ and $f_{ll}(k)$ are Fourier transformation of $G_{ll}(\omega)$ and $F_{ll}(\omega)$ in k -space. γ 's are the geometry factors:

- $\gamma(k)$: in-plane between A and B Ir atoms
- $\gamma_{AA}(k)$: Nearest layers between A-A or B-B Ir atoms
- $\gamma_{AB}(k)$: Nearest layers between A-B Ir atoms

The equation of motion was solved self-consistently for $T = 80$ K, which is our experimental temperature. Once the local correlation function,

$$\langle S_l^- S_l^+ \rangle = \frac{i}{2\pi} \int_{-\infty}^{\infty} \frac{d\omega}{e^{\frac{\omega}{k_B T}} + 1} \{g_{ll}(\omega + i0^+) - g_{ll}(\omega - i0^-)\} \tag{11}$$

is obtained from the closed self-consistent loop, the local magnetic moments $\langle S_l^z \rangle$ of each layer,

$$\langle S_l^z \rangle = \frac{1}{2} - \langle S_l^- S_l^+ \rangle \tag{12}$$

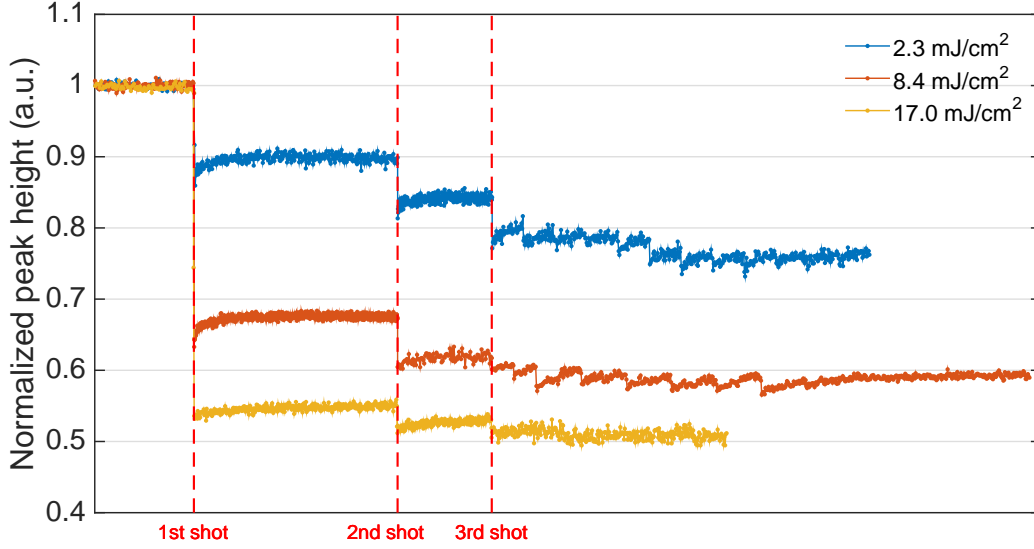


Fig. S 9: **Evolution of the magnetic peak height under excitation of multiple shots:** The pristine magnetic order was degraded by a sequence of single laser shots, the first three single shots were marked by red dashed lines. With increasing the laser fluence, the degree of the suppression of magnetic order keep reducing in the first initial stage where permanent suppression occurs; At high fluence, the multiple shots after the very first single shot drives marginal further suppression to the magnetic order and the system enters into a stable stage.

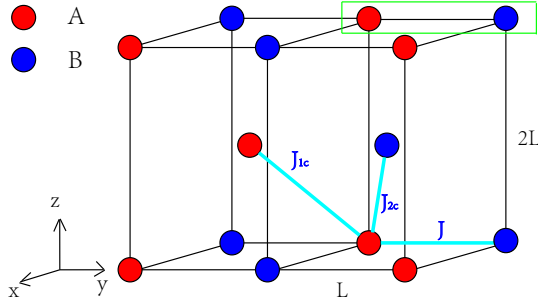


Fig. S 10: **Minimum model of an AFM ordered spin-1/2 system:** The ordered spins are grouped into the spin-up (A) and spin-down (B) sub-lattices. The exchange terms considered are labeled accordingly.

was extracted and plotted as **Fig. 4** in the main text.

-
- [1] C. Rayan Serrao, J. Liu, J. T. Heron, G. Singh-Bhalla, A. Yadav, S. J. Suresha, R. J. Paull, D. Yi, J. H. Chu, M. Trassin, et al., Epitaxy-Distorted Spin-Orbit Mott Insulator in Sr_2IrO_4 Thin Films, *Phys. Rev. B* 87, 085121 (2013).
 - [2] Q. Huang et al., Neutron Powder Diffraction Study of the Crystal Structures of Sr_2RuO_4 and Sr_2IrO_4 at Room Temperature and at 10 K, *J. Solid State Chem.* 112, 355 (1994).
 - [3] S. Fujiyama, H. Ohsumi, T. Komesu, J. Matsuno, B. J. Kim, M. Takata, T. Arima, and H. Takagi, Two-Dimensional Heisenberg Behavior of $\text{Jeff}=1/2$ Isospins in the Paramagnetic State of the Spin-Orbital Mott Insulator Sr_2IrO_4 , *Phys. Rev. Lett.* 108, 247212 (2012).
 - [4] S. J. Moon, H. Jin, W. S. Choi, J. S. Lee, S. S. A. Seo, J. Yu, G. Cao, T. W. Noh, and Y. S. Lee, Temperature Dependence of the Electronic Structure of the $\text{Jeff}=1/2$ Mott Insulator Sr_2IrO_4 Studied by Optical Spectroscopy, *Phys. Rev. B* 80, 195110 (2009).
 - [5] M. Dean, Y. Cao, X. Liu, S. Wall, D. Zhu, R. Mankowsky, V. Thampy, X. M. Chen, J. G. Vale, D. Casa et al., Ultrafast Energy- and Momentum-Resolved Dynamics of Magnetic Correlations in the Photo-Doped Mott Insulator Sr_2IrO_4 , *Nat. Mater.* 15, 601 (2016).

- [6] X. Liu, T. Berlijn, W.-G. Yin, W. Ku, A. Tsvelik, Y.-J. Kim, H. Gretarsson, Y. Singh, P. Gegenwart, and J. P. Hill, Long-Range Magnetic Ordering in Na_2IrO_3 , *Phys. Rev. B* 83, 220403(R) (2011).
- [7] H. Diep, Quantum Effects in Heisenberg Antiferromagnetic Thin Films, *Phys. Rev. B* 43, 8509 (1991).
- [8] A. Moschel, and K. D. Usadel, Magnetization of Coupled Ferromagnetic and Antiferromagnetic Films: Dependence on the Interface Coupling, *Phys. Rev. B* 48, 13991 (1993).
- [9] J. Porras, J. Bertinshaw, H. Liu, G. Khaliullin, N. H. Sung, J.-W. Kim, S. Francoual, P. Steffens, G. Deng, M. M. Sala, A. Efimenko, A. Said, D. Casa, X. Huang, T. Gog, J. Kim, B. Keimer, and B. J. Kim, Pseudospin-Lattice Coupling in the Spin-Orbit Mott Insulator Sr_2IrO_4 , *Phys. Rev. B* 99, 085125 (2019).
- [10] Y. Gim, A. Sethi, Q. Zhao, J. F. Mitchell, G. Cao, and S. L. Cooper, Isotropic and Anisotropic Regimes of the Field- Dependent Spin Dynamics in Sr_2IrO_4 : Raman Scattering Studies, *Phys. Rev. B* 93, 024405 (2016).
- [11] S. Calder, D. M. Pajerowski, M. B. Stone, and A. F. May, Spin-Gap and Two-Dimensional Magnetic Excitations in Sr_2IrO_4 , *Phys. Rev. B* 98, 220402(R) (2018).
- [12] D. Pincini, J. G. Vale, C. Donnerer, A. de la Torre, E. C. Hunter, R. Perry, M. Moretti Sala, F. Baumberger, and D. F. McMorrow, Anisotropic Exchange and Spin-Wave Damping in Pure and Electron-Doped Sr_2IrO_4 , *Phys. Rev. B* 96, 075162 (2017).
- [13] S. Bahr, A. Alfonsov, G. Jackeli, G. Khaliullin, A. Matsumoto, T. Takayama, H. Takagi, B. Büchner, and V. Kataev, Low-Energy Magnetic Excitations in the Spin-Orbital Mott Insulator Sr_2IrO_4 , *Phys. Rev. B* 89, 180401(R) (2014).
- [14] P. Fröbrich, and P. J. Kuntz, Many-Body Green's Function Theory of Heisenberg Films, *Phys. Rep.* 432, 223 (2006).